Characterization of supercooled droplet by Laser-Induced Fluorescence: Temperature and ice fraction

Mehdi Stiti, Alexandre Labergue, Fabrice Lemoine, Didier Stemmelen, Sébastien Leclerc

Characterization of supercooled droplet by Laser-Induced Fluorescence: Temperature and ice fraction

M. STITI[1*], A. LABERGUE[1], F. LEMOINE[1], D. STEMMELLEN[1], S. LECLERC[1]
1: Université de Lorraine, CNRS, LEMTA, F-54000 Nancy, France
* Correspondent author: mehdi.stiti@univ-lorraine.fr

Keywords: Laser Induced Fluorescence, Supercooled droplets, Water solidification, Raman, NMR

ABSTRACT

An extension and new application of the Laser Induced Fluorescence (LIF) is here developed for supercooled droplet characterization (temperature and solidification). In a first step, the choice of fluorescent dyes is determined by the study of fluorescent spectra at different temperatures. A couple of two fluorescent dyes has been identified allowing a temperature measurement. The water (with both dyes) was then calibrated in temperature using a suspended droplet up to a temperature of $-17°C$ and a sensitivity of $2.56\%/°C$ was obtained. The measurement technique is then used to determine the droplet temperature in free fall in a cold environment. An experimental setup consisting of a column with a height of $79cm$ whose internal temperature can be controlled up to a temperature of $-54°C$ is used. Two configurations of drops were tested: individual drops generated by a syringe pump and a mono-sized droplet chain. In parallel, numerical simulations were carried out for both configurations (taking into account the internal circulation of the liquid within the drops and the drop-drop interactions) possible to set up a second fluorescence ratio that is very sensitive to phase change. This second ratio was tested on a suspended droplet and in an experimental setup that allows a following of the phase change more precisely. It appears an almost proportional evolution between the evolution of the ratio and the evolution of ice in the water. Finally, measurements of Raman spectroscopy and MRI have been performed in order to confirm that LIF is a relevant technique to detect and estimate the ice fraction.

1. Introduction

The characterization of supercooled droplet is a largely covered topic, especially in the case of supercooled water droplets impacting onto a wall [1] [2] [3]. The solidification process of a supercooled drop exhibits different solidification phase [4]. The velocity of the ice front that is formed during the droplet freezing phase depends on many parameters required, such as the temperature of the impinging droplet, the velocity of the droplet or the nature of the material of the impacting surface. Ice accretion represents a severe hazard in transportation systems, especially in aviation. In order to validate ice tunnel tests, the characterization of supercooled droplets before the impact is needed. Characterization of supercooled droplet can be achieved by

different optical methods. The ILIDS (Interferometric Laser Imaging for Droplet Sizing) method makes it possible to measure mean size of ice crystals for supercooled drops [5], as Raman spectroscopy allows following of the phase change[6] [7]. NMR allows the measurement of the fraction of ice present in a droplet and a following of the phase change during the time [8] [9]. The simultaneous measurement of temperature and ice fraction by a non-intrusive technique was never achieved according to the best of our knowledge. The temperature measurement of droplet by LIF2c is well documented in the literature. Up to now, the method was mainly used in the case of droplets evolving in a hot environment and in the case of droplets impinging onto heated walls in the Leidenfrost regime [10] [11]. Therefore, the objective of the present study is to extend the application field of the LIF technique in the case of supercooled droplets and to estimate the ice fraction formed within the supercooled droplets.

2.1 Principle of two-color Laser Induced Fluorescence thermometry

The principle consists in dissolving an organic fluorescent dye at very low concentration in water. A laser excitation, tuned on the absorption spectrum of the dye molecule is provided and the resulting fluorescence signal is measured. The use of temperature sensitive fluorescence dyes makes then thermometry possible. The most widespread model of the fluorescent signal [9] can be rearranged by introducing the sensitivity in temperature of the dye (s in $\%/°c$). This sensitivity is assumed depending only on the dye and not on the temperature. The fluorescent signal I_{fi}, collected on a given spectral band i in a measuring volume V_c , at a temperature T, can be written as:

$$I_{fi}(T) = K_i . c . V_c . I_0 . e^{s_i . T} \quad (1)$$

With I_0 the local laser excitation intensity, c the fluorescent dye concentration and K_i a constant depending on both the dye and the optical chain detection. Both parameters I_0 and V_c being generally difficult to determine, they can be removed by collecting simultaneously the fluorescent signal on two spectral band I_{f1} and I_{f2} in order to derive a ratio $R_{12} = \frac{I_{f1}}{I_{f2}}$. This method is referred as two colors, one dye LIF (LIF2c1d). For a method with two dyes seeded in the fluid (LIF2c2d), the ratio can be expressed as:

$$R_{12} = \frac{I_{f1}}{I_{f2}} = \frac{K_1 . c_1}{K_2 . c_2} . e^{(s_1 - s_2) . T} \quad (2)$$

Finally a reference R_{120} at a known temperature (T_0) may be used to remove the constant K_i and c_i. Therefore, a normalized ratio can be obtained:

$$\frac{R_{12}(T)}{R_{120}(T_0)} = e^{(s_1 - s_2) . (T - T_0)} \quad (3)$$

As shown in the equation (3), the knowledge of the sensitivity in temperature ($s_1 - s_2$) allows a temperature measurement. This parameter is obtained by a calibration in temperature (*see section 2.4*). Moreover, it assumed that the concentrations of the fluorescent dyes are not dependant on the temperature.

2.2 Study of different fluorescent dyes

The novelty of this works lies in the temperature measurement of supercooled water, which was never done according to the best of our knowledge. Therefore, the first step is to test several fluorescent dyes in order to find the one having the best temperature sensitivity in the case of supercooled water. The following dyes Rhodamine B (Rhb), Rhodamine 560 (Rh560), Eosin (Eo) and Kitonred (Kr) were seeded in water and their fluorescent spectra at different temperature were studied.

2.2.1 Experimental setup

The study of the fluorescent dyes is carried out in a cell of 600µL (Fig 1). The cell is inserted between two heat exchangers (**Fig. 1**) inside which a coolant fluids flows and is controlled in temperature by a refrigerant supply (LAUDA ®). This device allows a volume cooling of the water and is also equipped of optical accesses for fluorescence measurements. The fluorescence is induced by the green line of a continuous laser (λ=532nm, Ventus Laser Quantumn) and the fluorescence spectra are recorded with a spectrometer (StellarNet Inc with a resolution of 0.4nm). A measurement of the water temperature is performed by a thermocouple inserted in the cell.

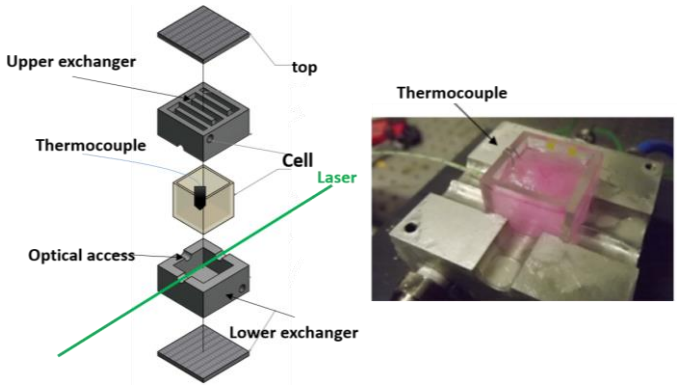

Fig. 1 Experimental setup for the characterization of fluorescent dyes seeded in water

The measurement consists on the study of the spectra of the different fluorescent dyes at different temperatures.

2.2.2 Results

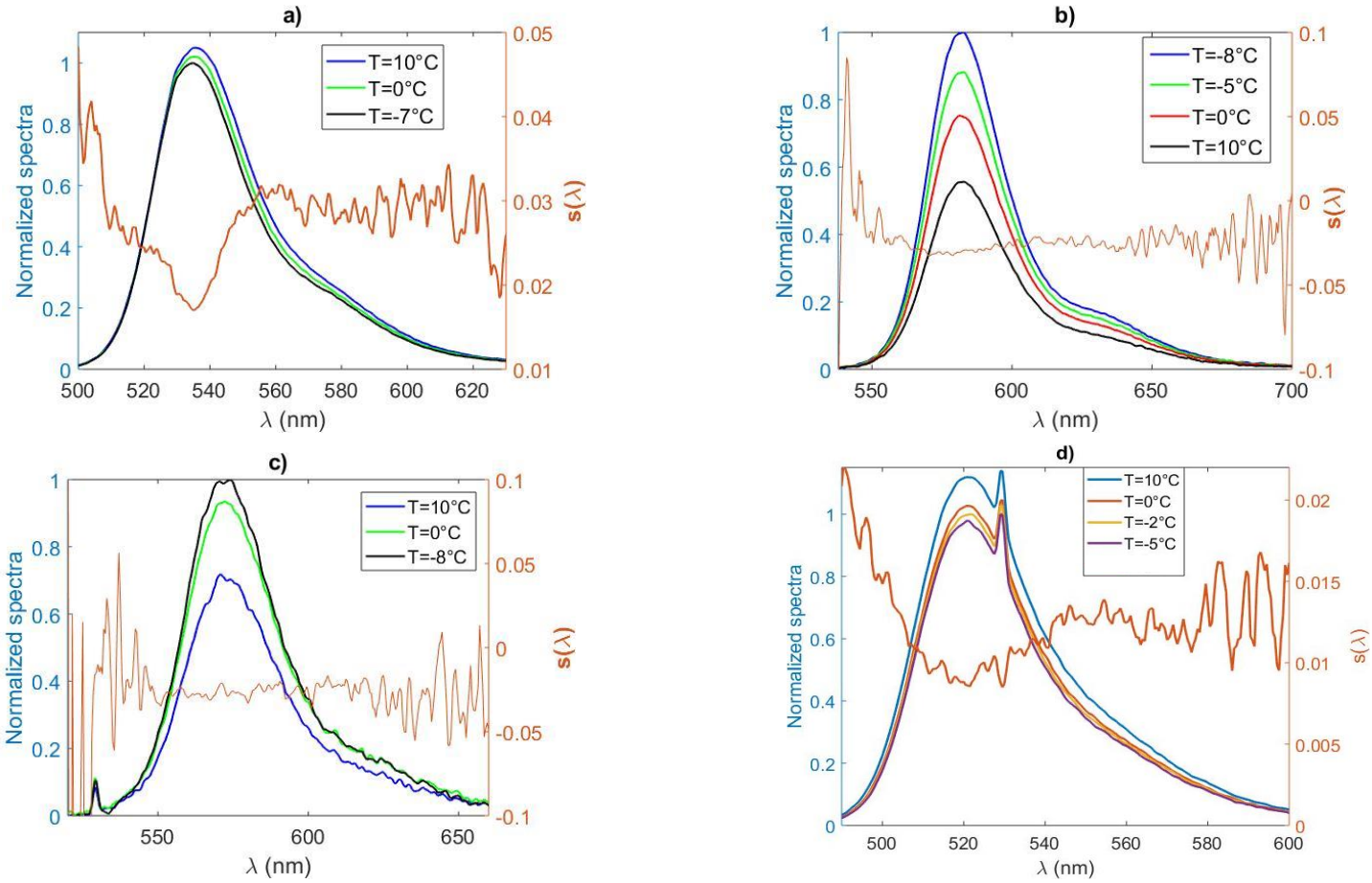

Fig. 2 Typical spectra (left axis) at different temperatures normalized with the lowest temperature and temperature sensitivity (right axis) as a function of the wave-length for Eo (a), KR (b), RhB (c) and Rh560 (d).

Typical spectra of tested fluorescent dyes are reported on **Fig. 2**, Eosin (a), Kitonred (b), RhodamineB (c) and Rhodamine560 (d) with molar concentration of $c_{Rhb} = 10^{-5} mol.L^{-1}$, $c_{Kr} = 10^{-6} mol.L^{-1}$, $c_{Eo} = 10^{-5} mol.L^{-1}$ and $c_{Rh560} = 10^{-5} mol.L^{-1}$ respectively.

One can observe:

- An increase of the fluorescent intensity when the temperature decreases in the case of Rhb and Kr. For both dyes, the temperature sensitivity is about 2.3%/°C [12] on the entire spectra. The fluorescent intensity depends essentially of the quenching and not on the temperature dependency of the absorption.
- The Eosin sees its fluorescence signal increases when the temperature decreases and has a temperature sensitivity of about 3%/°C on the entire spectra.
- The Rhodamine 560 sees its fluorescence signal decreases when the temperature decreases. This increasing is mainly due to the increasing of the absorption cross section 532nm with

the temperature [12] [13] The temperature sensitivity is about +0.78%/°C on the entire spectra.

In order to increase the temperature sensitivity of our solution, the use of two dyes has been investigated.

2.3 Temperature measurement by LIF2c2d

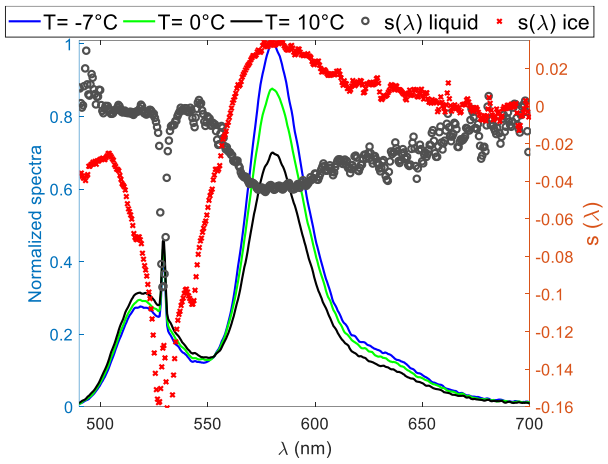

Fig. 3 Typical spectra of the Kr/Rh560 mixture (left axis) for different temperatures normalized by the value at the lowest temperature and evolution of the temperature sensitivity (right axis) as a function of the wavelength for solid (ice) and liquid phases.

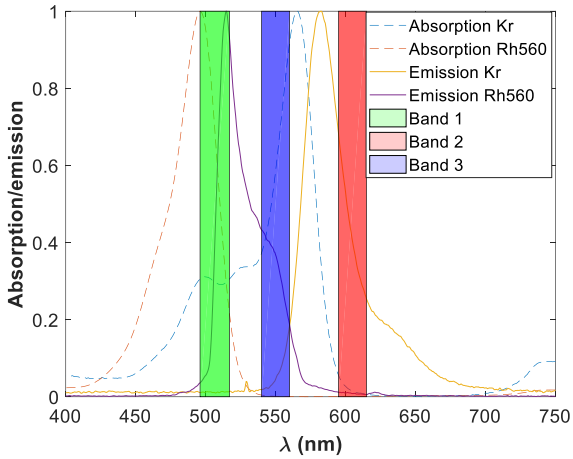

Fig. 4 Representation of the selected spectral bands of detection for the LIF3c2d technique

Following tests on a single dyes solution oriented our work toward a solution with two dyes seeded in the water. Taking into account the water solubility, the final solution used Rh560 ($c_{Rh560} = 0.5.10^{-5} mol.L^{-1}$) and Kr ($c_{Kr} = 0.5.10^{-6} mol.L^{-1}$). The **Fig. 3** presents typical spectra of the solution recorded at different temperatures (from $10°C$ to $-7°C$) and normalized by the value at the lowest temperature. It can be clearly observed that the two dyes have different temperature dependences, the temperature sensitivity of Kr being significant (order of -2.4%/°C) this of the Rh560 being very low (order of +0.8%/°C). Consequently, the combination of these two dyes for designing a ratiometric technique should lead to a high temperature sensitivity.

According to equation (3), improving the temperature sensitivity means selecting two spectral bands of detection that present a maximized difference ($s_1 - s_2$). This step may be performed by analyzing the evolution of the temperature sensitivity as a function of the wavelength (***Fig. 4***), the selected spectral bands are:

- Band 1: [496-517] nm: only Rh560 has a contribution in this band, the fluorescence intensity decrease with the decrease of the temperature. Furthermore, fluorescence is partially absorbed by the Kitonred and self-absorbed.
- Band 2: [595-615] nm: only Kr has a contribution in this band, the fluorescence intensity increase when the temperature decreases.

However, it is also necessary to take into account the absorption of a dye by the other one (Type II spectral conflict [12]) that may depend on the temperature as well as on the optical path length. The absorption and emission spectra of each dye are represented in **Fig. 4**. It appears that the band 1 may lead to such a spectral conflict: the Rh560 emission may be self-absorbed and absorbed by the Kr. However, in [13], the authors show that the absorbance of the Kr does not depend on the temperature, which makes it possible to safely neglect this conflict. Moreover, in this work, LIF2c2d is applied to droplets where path lengths are very low (approximately $100\mu m$) which leads the re-absorption phenomena negligible.

2.4 Temperature calibration

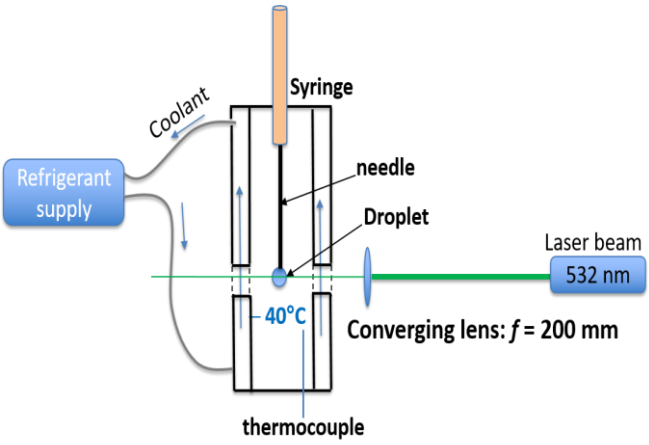

Fig. 5 Calibration setup on a suspended droplet

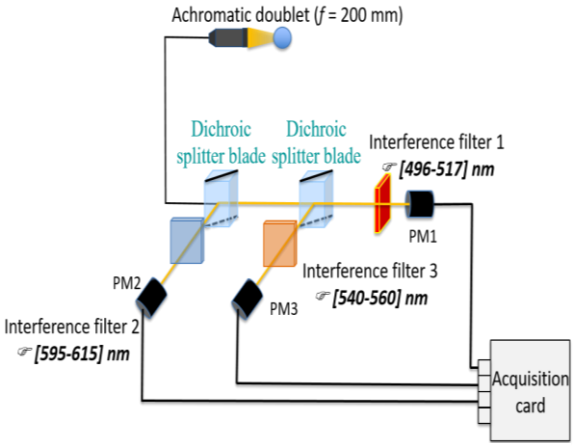

Fig. 6 LIF optical setup

The difference $(s_1 - s_2)$ in the equation (3) can be obtained by a preliminary calibration that consists to measure the ratio R_{12} at different controlled temperatures. The calibration was performed on a suspended droplet by using the experimental setup depicted in **Fig. 5** The setup consists of a chamber equipped with a double envelope cylinder ($185mm$ of height and $80mm$ inner diameter) in which a circulation of a coolant fluid (Thermal HL80) is established, the temperature of which being controlled by a supply chiller system (Julabo presto®). With this system, it is possible to control the temperature in the chamber between $+70°C$ and $-45°C$. The fluorescence is induced by a CW double Nd-Yag laser ($\lambda = 532nm$, Ventus LaserQuantum®). The

laser beam is focused within the droplet with the use of a converging lens (focal length of $f = 200mm$) in order to increase the excitation power density and then to improve the signal/noise ratio of the fluorescence signal. The droplet (approximately $2mm$ in diameter) is suspended on a needle (outer diameter of $400\mu m$). A thermocouple placed close to the droplet allows air temperature in the chamber to be measured. The measurements are acquired step by step after the thermal equilibrium between the air and the droplet is attained. The equilibrium time can be estimated by $20sec$ and, to assure the temperature equilibrium, each point are acquired after $5min$. The fluorescence signal is collected at right angle by means of an achromatic doublet (focal front lens of $200mm$) and coupled with an optical fiber having a core diameter of $70\mu m$. The collected fluorescence signal is splited into the two selected spectral by means of a set of dichroic and interference filter (**Fig. 6**). The fluorescence is detected by means of two photomultiplier tubes, transformed into a voltage by means of a trans impedance converted, digitalized and acquired on a computer. **Fig. 7** presents the temperature calibration curve: evolution of $ln(\frac{R_{12}}{R_{120}})$ as a function

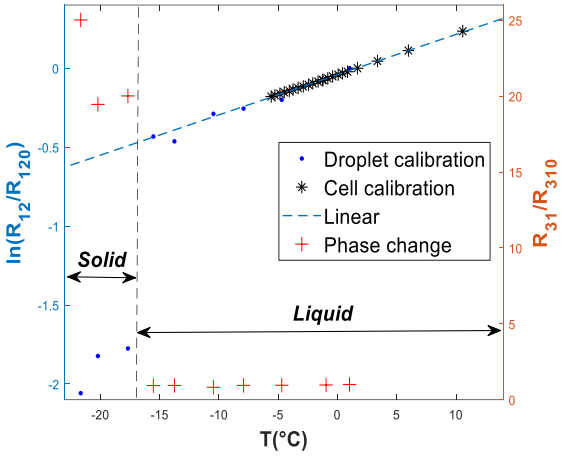

Fig. 7 Left axis: Temperature calibration obtained in the case of a suspended droplet and comparison with results obtained in a cell. Right axis: evolution of the logarithm of the second normalized fluorescence ratio measured in the case of a suspended droplet

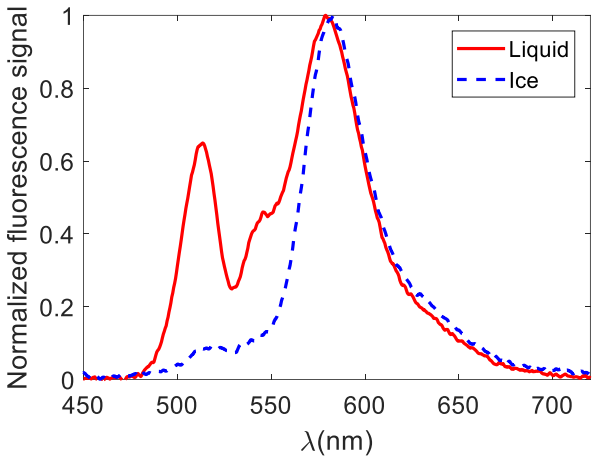

Fig. 8 LIF spectra of Kr/Rh560 dissolved in liquid and frozen water.

of the air temperature, where the reference ratio R_{120} is taken at $T_0 = 0°C$.
Two trends can be clearly observed with a break of for $\ln\left(\frac{R_{12}}{R_{120}}\right)$ observed around $-17°C$. It corresponds to the droplet freezing, which is confirmed by a simple visual control (because laser light is scattered by the presence of ice). Further discussions and comments about this phenomenon will discussed be in *section 3*, especially the presence of a second fluorescence ratio $\frac{R_{31}}{R_{310}}$ will be justified. In the liquid and supercooled phases, a sensitivity of $2.56\%/°C$ is obtained.

Due to the choice of the spectral bands, we do not find exactly the sum of the sensitivities of each dyes. To check the validity of the calibration, similar measurements are performed using the setup of **Fig. 2**. With this device, the supercooled state can be generally observed in a narrower temperature range than in the case of the suspended droplet due to the presence of the walls and the thermocouple. The measurements obtained in the cell, added in **Fig. 7** (black stars), agree well with those obtained in the suspended droplet. Note that the signal measured after the droplet freezing will induce erroneous measurements. It is then required to detect the phase change of water, which will be the object of section.

3.1 Influence of the phase change

It was found that the freezing of the droplet involves a change in the fluorescence emission (as seen in **Fig. 7** and **Fig. 8**). This can be potentially exploited to detect the phase transition and to evaluate the ice fraction present in the droplet. Indeed, it appears that the freezing involves a strong deformation of the fluorescence spectrum in the vicinity of the spectral region centered at 520nm (which justify the choice of the first selected band). Therefore, the use of a spectral band centered near $520nm$ can provide information on the phase change and on the presence of ice. More precisely, by using the first band of detection ($[496-517]nm$ this spectral band being the most modified by the freezing phenomenon) and a third spectral band ($[595-615]nm$), which is merely affected by the phase change, a second fluorescence ratio R_{31} can be derived that depends essentially on the presence of ice in the fluid and not on the temperature. The technique used now is referred as LIF3c2d. Measurements on a suspended droplet were undertaken in order to measure the evolution of the fluorescence ratio R_{31} as a function of the temperature. The results reported in the **Fig. 7** (red cross symbols) show that the normalized ratio $\frac{R_{31}}{R_{310}}$ is very few temperature dependent until the water remains in the supercooled state (liquid). When the freezing occurs (for temperature below $-17°C$ in **Fig. 7**), a strong raise of R_{31} can be observed, which is confirmed by visual control. Thus, the use of the second ratio R_{31} allows detecting whether the fluid contains ice or not.

3.2 Estimation of the ice fraction within supercooled water by LIF3c2d

The sensitivity to the phase highlighted in the last section opens the perspective to use the second fluorescence ratio R_{31} to determine the ice fraction within a supercooled droplet. The general idea is to determine a relationship between the value of the ratio R_{31} and the ice fraction. It consists in

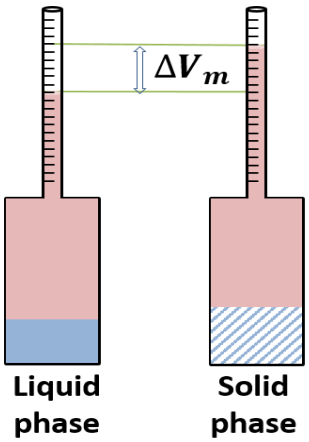

Fig. 9 Test cells used to monitor the phase change (freezing)

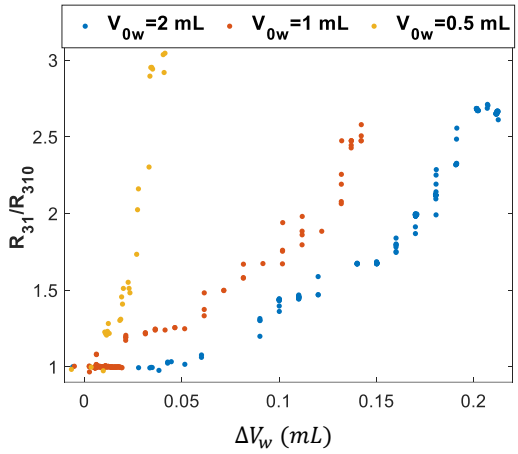

Fig. 10 Evolution of the normalized fluorescence ratio as a function the water volume variation.

establishing a second calibration curve that relates R_{31} to the ice fraction during the freezing phase. Due to the small water volume of the droplets used in the previous study (droplet of approximately 2 mm in diameter), it was not possible to observe thoroughly the transient phase change. Since ice apparition is correlated to a volume variation, a dedicated experimental setup that allows monitoring the evolution of the ice fraction within the fluid as a function of the ratio R_{31}, was developed. For that purpose, a special cell was built-up (**Fig. 9**): a graduated tube is mounted in the cell in order to measure the volume change due to the ice formation. An initial and known volume V_{0w} of water is placed in the cell and a volume V_{0c} of a coolant fluid (non-miscible with water and less dense than water) is added above the water up to around the middle of the graduated tube. The evolution of ice formation in the cell is deduced from the measurement of the global volume variation ΔV_m, measured by the graduated tube including the coolant volume variation. The tube cross-section is taken small enough compared to the cell cross-section in order to increase the sensitivity of the measurement (error on the order of $10^{-2}mL$) during the freezing process. The global volume variation ΔV_m at a given temperature T can be split in two terms:

$$\Delta V_m(T) = \Delta V_w(T) + \Delta V_c(T) \quad (4)$$

where ΔV_w and ΔV_c are the volume variations of the water and the coolant respectively. Due to the expansion of the coolant with the temperature ($k_c = 9.7 * 10^{-4}K^{-1}$), a correction on the coolant volume measurement (ΔV_c) is calculated according to:

$$\Delta V_c(T) = k_c.(T - T_0).V_c(T_{0c}) \quad (5)$$

where T_{0c} being the initial temperature of the coolant and V_{0c} the initial volume. The measurement of the fluorescent signal is done by the same setup as the previous one (**Fig. 6**) and is synchronized with a camera to monitor the volume variation ΔV_{0c}. In order to improve the measurement (ice transparency and supercooled degree), the cell is first heated (up to $70°C$) to evacuate the air dissolved in the water and in the coolant. Then, the cell is cooled down slowly, which allows obtaining a relatively transparent ice. The **Fig. 11** represents a typical volume variation (ΔV_m) during an experiment. The experiments were carried out for three different initial water volumes V_{0w}. The evolutions of the fluorescent ratio $\frac{R_{31}}{R_{310}}$ as a function of the water volume variation ΔV_w are presented in **Fig.10**. As in the droplet study (**Fig. 7**), the fluorescent ratio $\frac{R_{31}}{R_{310}}$ remains constant

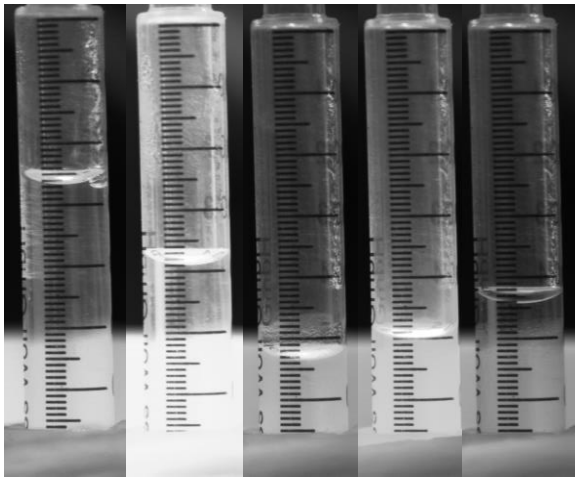

Fig. 11 Typical volume variation during an experiment. t_{heat}, t_{init}, t_{cool}, t_{sol} represent images taken during the heating, the cooling and solidification process.

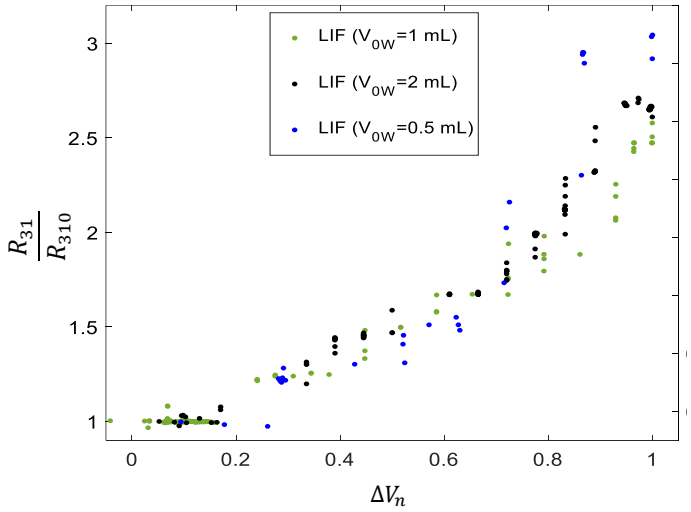

Fig. 12 Evolution of the normalized fluorescent ratio and Raman ratio as a function of the normalized water volume variation

in the liquid phase and when ice appears a progressive increase of $\frac{R_{31}}{R_{310}}$ can be observed. For each of the initial water volumes, it reaches an approximate same maximum value corresponding to the solid phase. The value obtained when the water is totally frozen differs according to the type of ice formed. In the cell experiments (**Fig. 9**), a relatively clear ice is obtained as more opaque ice is observed in the case of droplet (**Fig. 5**). To be sure that the solidification process is independent of the initial volume V_{0w}, the evolution of the water volume was normalized by the water volume corresponding to 100% of ice $\Delta V_w(ice)$. This volume was obtained with **Fig. 10** when the ratio R_{31} reaches its maximum value. **Fig. 12** describes the evolution of the normalized fluorescence ratio as a function of the normalized water volume $\Delta V_n = \frac{\Delta V_w}{\Delta V_w(ice)}$ and it appears that all the plots are

almost superposed, the highest uncertainty being found for the smallest water volume $V_{0w} = 0.5\ mL$.

4. Comparisons of LIF technique with Raman spectroscopy and MRI

In order to validate the measurement of ice fraction by LIF technique, a comparison with Raman and MRI spectroscopy is made.

4.1 Raman measurements

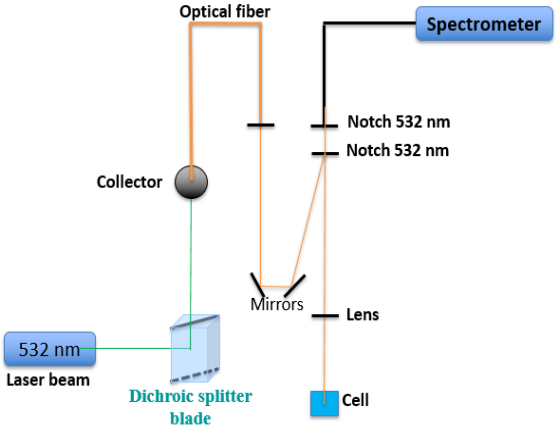

Fig. 13 Optical setup for the Raman study

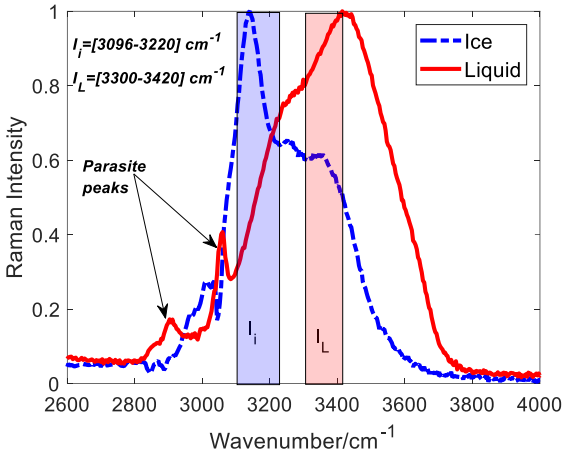

Fig. 14 Raman spectrum of ice and water and the different spectral bands used for the evaluation of $S_{I/L}$.

Raman spectroscopy is a relevant method for the investigation of the composition of a fluid due to the high sensitivity of the Raman spectra to the molecular environment [14] [15]. By studying the Raman spectra of a fluid, the different vibrational peaks of the spectrum are the signature of the molecules that are present in the fluid. In the case of the solidification of water, it was demonstrated that Raman spectroscopy could be used to detect the phase transition [6], [7] when the OH-stretching band corresponding to $[2800 - 3800] cm^{-1}$ (for an excitation with CW double Nd-Yag laser $\lambda = 532nm$) is considered. For this study, a Raman spectroscopy device by retro diffusion was setup (**Fig. 13**). It can be seen that the Raman spectra for both liquid and solid phases of water are slightly different. The parasite peaks in the Raman spectrum (**Fig. 14**) are due to the material that composed the cell. By quantifying the deformation of the Raman spectra, it is possible to determine two spectral bands that are sensible to the phase change. To investigate the phase transition, a ratio $S_{I/L}$ that corresponds to the ratio of the spectral band corresponding to the solid

phase (I_i) and the band corresponding to the liquid phase (I_l) [6] was calculated. The two spectral bands selected for this study are:

- $I_i = [3096 - 3220] cm^{-1}$
- $I_l = [3300 - 3420] cm^{-1}$

From **Fig. 16** (orange cross), it can be observed that the ratio $S_{I/L}$ increases during the solidification process as for LIF measurement.

4.2 MRI measurements

Magnetic Resonance Imaging is also a methode able to distinguish the ice fraction in a mixture of liquid water and ice. The principle of measurement of the ice fraction is relatively simple and uses the fact that the Nuclear Magnetic Resonance relaxation times are very short, some μs, for solids, whereas they can reach several seconds for liquids [8], [9]. In other words, the Magnetic Resonance signal corresponding to the ^{1}H of the ice disappears very rapidly while the one corresponding to the ^{1}H of liquid water persists over a period of the order of magnitude of the second. The decrease of the ^{1}H MRI signal during the solidification process of the water therefore gives direct access to the ice fraction. It is simply necessary to choose a sufficiently long MRI echo time (at least a few ms) in order to not detect the signal coming from the ice.

Measurements were performed on a wide-bore 600 MHz NMR spectrometer equipped with an MRI imaging system. To obtain the change in volume during the solidification period, the same device of **Fig. 9** was used. The cell was cooled inside the NMR magnet by means of a cold air flow (up to $-40°C$) controlled in temperature. MRI images were acquired to follow the displacement of the interface between the water and the coolant fluid, representative of the change in volume of the water during its solidification. The MRI sequence used is a RARE [9] sequence with an echo time of 3 ms, an echo train length of 32 and a repetition time of 1s. The field of view of the images is $4 * 4cm$, with a mtrix of $256 * 256$ $pixels$. The NMR measurements are made on a vertical section of thickness 2 mm centered in the middle of the cell.

The ^{1}H of the water and coolant fluid do not resonate exactly at the same frequency which leads to a chemical shift artifact, i.e a shift between the areas filled with water and those filled with coolant fluid (intermediate zone in white on the image of the **Fig. 15**). The displacement of the interface was then measured following the zone relating to the coolant fluid, undisturbed by the effects of phase change. Exemples of normalized MRI images (Im_n) are presented in **Fig. 15.** The images (Im) are normalized using an image taken when the cell contains only liquid (ref). This normalization aims to substract the effect of non-homogeneity of the magnetic gradients. The normalized images are then:

$$Im_n = \frac{Im(t) - ref}{ref} \tag{6}$$

Therefore the ice fraction (X_I) is then calculated using the two zone (**Fig. 15**):

$$X_I = \frac{V_{(1+2)}(ice)}{V_{(2)}(liquid)+V_{(1+2)}(ice)} \quad (7)$$

where $V_{(1+2)}(ice)$ is the volume of ice in the zone 1 and 2. Moreover, from Fig. 15, one can oserve the ice formation in blue. In **Fig. 16** (red stars), are indicated the MRI measurements of the solid fraction as a function of the normalized water volume variation during the solidification process.

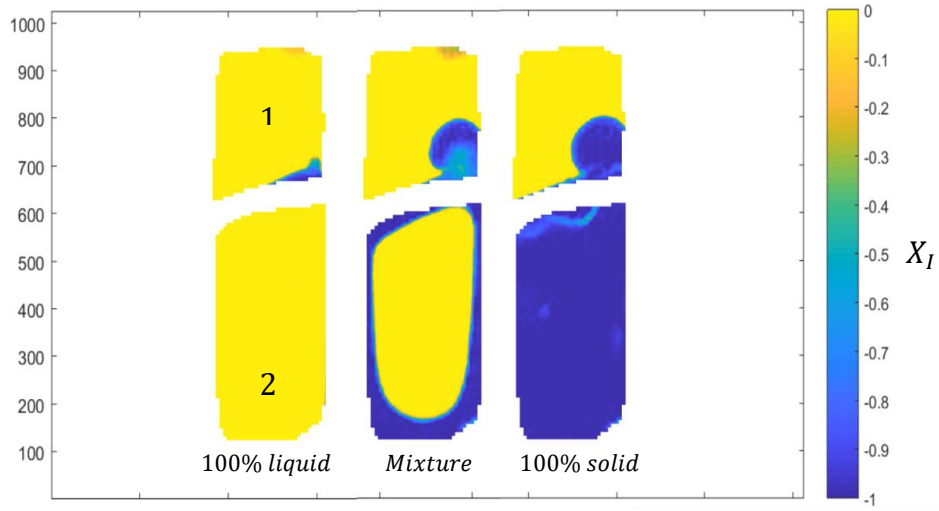

Fig. 15 MRI Images of the water solidification in the cell. Zone 1 corresponds to the coolant part and zone 2 to the water part.

4.3 Comparisons

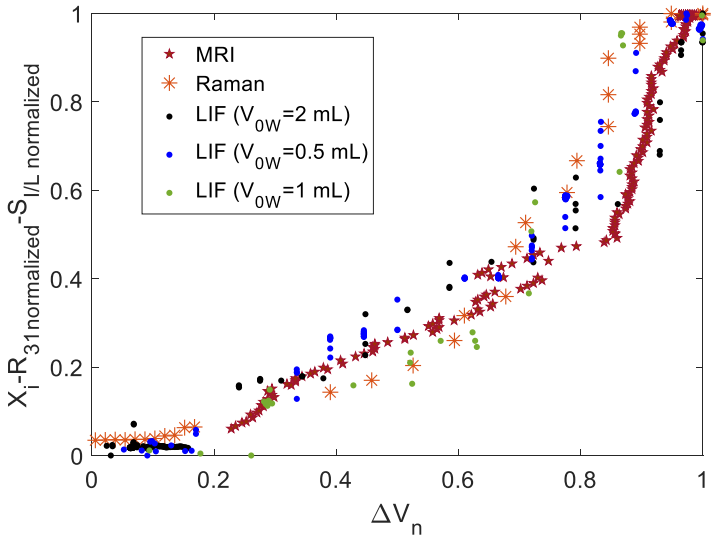

Fig. 16 Evolution of the normalized fluorescent ratio, Raman ratio and ice fraction (MRI) as a function of the normalized water volume variation

Each measurement are normalized between 0 and 1 in order to compare all techniques. The normalized value are $\frac{R_{31}}{R_{310}n}$ and I_{I/L_n} for LIF measurement and Raman spectroscopy respectively:

$$\frac{R_{31}}{R_{310_n}} = \frac{\frac{R_{31}}{R_{310}} - \min\left(\frac{R_{31}}{R_{310}}\right)}{\max\left(\frac{R_{31}}{R_{310}}\right) - \min\left(\frac{R_{31}}{R_{310}}\right)} \; ; \; I_{I/L_n} = \frac{I_{I/L} - \min(I_{I/L})}{\max(I_{I/L}) - \min(I_{I/L})} \quad (8)$$

The **Fig. 16** represents the evolution of the normalized fluorescent ratio, Raman ratio and ice fraction (MRI) as a function of the normalized water volume variation. We can observe that LIF and Raman measurements give rise to similar trend with a quite good overlap of the measurements. As Raman spectroscopy being validated to monitor the phase change, we can confirm that LIF techniques allow monitoring the phase change.

As for Raman spectroscopy, a good overlap of MRI and LIF measurements is observed. As MRI technique allows an exact determination of the ice fraction in water, we can then use the LIF techniques to determine the ice fraction presents in supercooled water.

5. Measurements on supercooled droplet falling in a cold environment

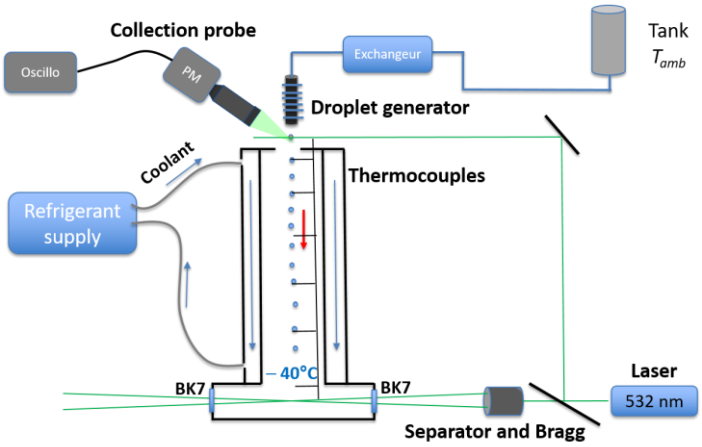

Fig. 17 Experimental setup : single droplets of falling droplets in a cold environment.

The test of the technique LIF3c2d is performed on supercooled droplets evolving in a cold environment. The setup used to cool down the droplets is presented **Fig. 17**. It consists in cylindrical enclosure equipped with a double envelope, of 790 mm high and 110 mm in diameter. A coolant flows in the double envelope in order to control the temperature of the air within the enclosure. The temperature of the air (T_{amb}) inside the enclosure is measured. At the bottom of the column, 4 BK7 windows allow optical measurements. The measurement zone is located at the intersection volume of two converging laser and focuses laser beams (as in LDA device) at $79cm$ from the droplet injection point and is centred on the main vertical axis of the column.

5.1 Measurements on single droplets

Single droplets (diameter of 2.5mm) are generated using a needle (400μm) connected to a syringe pump. The injection temperature T_{inj} of the droplet is controlled by a heat exchanger and measured by a thermocouple inserted in the needle. Experiments were compared with a model based on those developed by Abramson and Sirignano [16] with the use of effective diffusion to model the heat transfer within the droplet and Ranz-Marshall correlation for calculating the heat transfer coefficient:

$$Nu = \frac{h.D}{k_a} = 2 + 0.6 * Pr^{\frac{1}{3}}.Re^{\frac{1}{2}} \quad (9)$$

Where D is the droplet diameter and k_a the thermal conductivity of the ambient air and h the convective heat transfer coefficient at the surface of the droplet. The temperature T_n, obtained by numerical simulation, is calculated on a duration that corresponds to the flight time of the droplets to reach the measurement volume position inside the column. This duration is about 400ms. The simulations are performed using the software COMSOL Multiphysics. The **Fig. 18** displays both

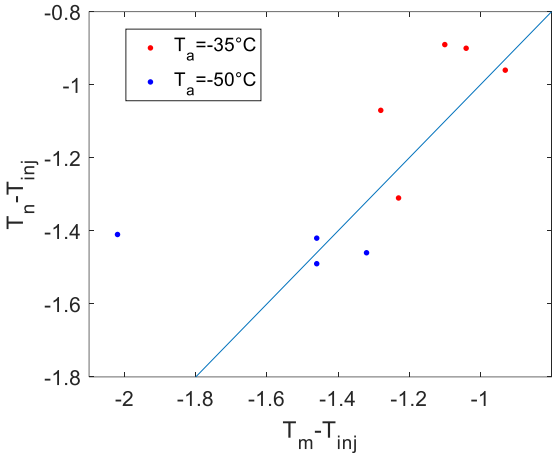

Fig. 18 Comparison between of thebetween the measured and simulated temperaturetemperatures measurement on afor singlefor single droplets of 2.5mm in diameter.

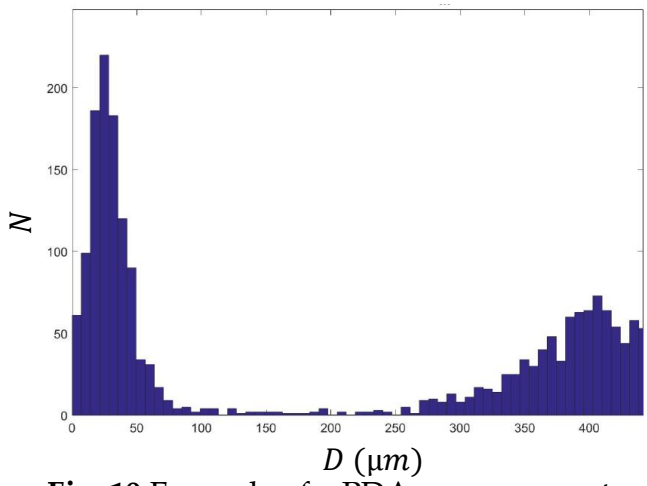

Fig. 19 Example of a PDA measurement with a membranne diameter of 200µm.

experimental and numerical results for different ambient temperature (T_{amb}) and different injection temperatures. For both cases, experiments and simulation, the cooling ($T_m - T_{inj}$) and ($T_n - T_{inj}$) respectively are about $-2°C$. This low cooling are is due to the large diameter of the droplets. However, a good agreement between the experiments and the simulation can be observed, with an average error of 0.2°C.

5.2 Measurements with a monodisperse droplets stream

To generate small droplets, a monodisperse injector is used. By controlling the excitation frequency of a piezo ceramic element, the vibration disintegrates into droplets a liquid jet forced into a membrane orifice (diameter D_m). An optimal choice of the excitation frequency allows obtaining monodisperse droplets. The monodispersity is controlled by a fluorescence measurement, by checking the periodicity of the signal performed close to the injector exit (see **Fig. 17**). The height of the column leads impossible to keep the periodicity and monodispersity of

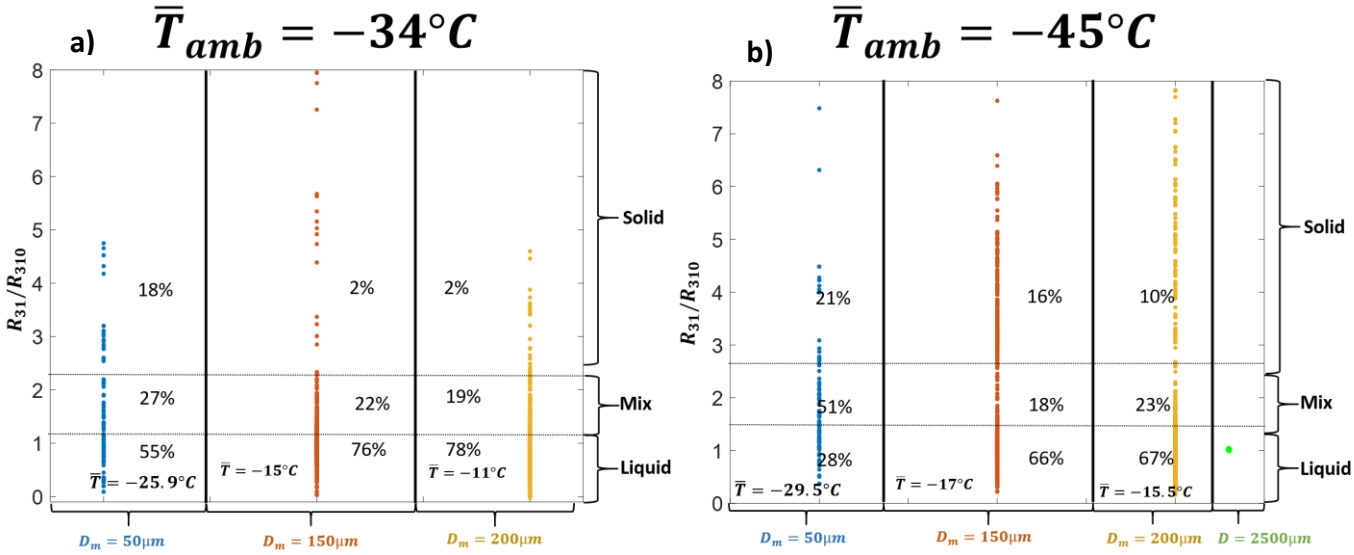

Fig. 20 Characterization of super-cooled droplets in a cold environment for two different ambiant temperature.

the droplets at the measurement point, due to coalescence or secondary atomization of the droplets. An example of PDA measurement is presented **Fig. 19** and we can clearly see that the droplets are not monodisperse. The results are then presented in function of the ratio R_{31} for different membrane diameters (D_m). **Fig. 20** represents the ratio $\frac{R_{31}}{R_{310}}$ measured for different membrane diameters and for 2 different ambient temperature controlled by the use of the 6 thermocouples placed along the column. The data corresponding to the single droplet case ($2500\mu m$ in diameter) for $T_{amb} = -45°C$ are added (green point) for which the injection temperature was 7°C. According to the result of **Fig. 16,** it was decided to decompose the state of the droplet (liquid, liquid/solid, frozen) according to the value of $\frac{R_{31}}{R_{310}}$:

- $\frac{R_{31}}{R_{310}} < 1.2$: liquid, supercooled droplet
- $1.2 < \frac{R_{31}}{R_{310}} < 2.45$: blended liquid/solid
- $\frac{R_{31}}{R_{310}} > 2.45$: frozen droplet

The percentage represented in **Fig. 20** corresponds to the fraction of droplets in the three states (calculated with an average number of 1000 droplets). It can be noted that when the droplets are not purely liquid, the temperature measurements (based on R_{12}) have to be taken with extra care,

due to the very inaccurate calibration of the fluorescence ratio as a function of the temperature. The droplet temperature is directly obtained by converting the value of the ratio R_{12} into temperature when droplet are purely liquid. The value $\bar{T}$ represents the mean temperature of the droplet in the liquid phase for different membrane diameters. We can note that the decreasing of D_m is equivalent to reduce the droplet's diameter. We can first observe that for a constant ambient temperature the proportion of purely liquid droplets decreases with the droplet diameter. Indeed, the smaller the drops are, the more they will tend to cool quickly and so they will have more chance to solidify. By regarding the temperature of purely liquid droplets in the case **a)** for example, we observe well that the temperature of the smallest droplets is $-25.9°C$ whereas the biggest droplets temperature is $-11°C$.

By comparing the case **a)** and **b)**, we observe well that the proportion of purely liquid droplet is decreasing while the proportion of frozen and blended droplets are increasing. For $D_m = 50\mu m$, we observe that the proportion of purely liquid droplets goes from 55% to 28%.

The last observation regarding to the result in **Fig. 18** is that smaller droplets ($D_m = 50\mu m$) remains liquid for lower temperature than in the case of larger droplets ($D_m > 50\mu m$), which agrees with previous results [17].

Conclusions

In this experimental study, a new ratiometric LIF technique using two dyes and three spectral bands of detection LIF3c2d was developed to both measure the temperature of supercooled droplets and obtain an estimation of the ice fraction. The temperature measurements are based on a ratio on two spectral bands that have different sensitivity into temperature. The use of a second ratio allows determining the state of the fluid: purely liquid, totally frozen or composed by a mixture of liquid and solid water. The comparison between LIF and both Raman and MRI measurements confirms that LIF technique is able to measure and detect the icing process of the water. To improve the comparison between LIF measurements and the data from a model [18] with a monodisperse stream experiment, a shorter column will be designed. The fly time of the droplets will be reduced and we will keep a constant and known diameter in the measurement volume. In order to quantify the ice fraction within a supercooled droplet during the freezing process, MRI measurements will be continued and will be compared to both LIF and Raman measurements on droplets.

Acknowledgements

The authors thank the French National Agency for its financial support through the project ANR ASTRID NUAGE (N°. ANR-15-ASTR-0003-01).

References

[1] M. Schremb, T. Webert, and C. Tropea, 'Experimental Investigation of Supercooled Water Drops Impacting onto a Smooth Ice Surface: Interaction of Fluid Flow and Phase Change', p. 13, 2017.
[2] T. Maitra, C. Antonini, M. K. Tiwari, A. Mularczyk, and Z. Imeri, *Supercooled Water Drops Impacting Superhydrophobic Textures*. .
[3] C. Zhang and H. Liu, 'Effect of drop size on the impact thermodynamics for supercooled large droplet in aircraft icing', *Phys. Fluids*, vol. 28, no. 6, p. 062107, Jun. 2016.
[4] M. Schremb and C. Tropea, 'Solidification of supercooled water in the vicinity of a solid wall', *Phys. Rev. E*, vol. 94, no. 5, Nov. 2016.
[5] M. Brunel *et al.*, 'Instrumentation for ice crystal characterization in laboratory using interferometric out-of-focus imaging', *Rev. Sci. Instrum.*, vol. 88, no. 8, p. 083108, Aug. 2017.
[6] I. Đuričković, R. Claverie, P. Bourson, M. Marchetti, J.-M. Chassot, and M. D. Fontana, 'Water–ice phase transition probed by Raman spectroscopy', *J. Raman Spectrosc.*, vol. 42, no. 6, pp. 1408–1412, Jun. 2011.
[7] X. Xue, Z.-Z. He, and J. Liu, 'Detection of water–ice phase transition based on Raman spectrum', *J. Raman Spectrosc.*, vol. 44, no. 7, pp. 1045–1048, Jul. 2013.
[8] J. P. Hindmarsh, A. B. Russell, and X. D. Chen, 'Measuring dendritic growth in undercooled sucrose solution droplets', *J. Cryst. Growth*, vol. 285, no. 1–2, pp. 236–248, Nov. 2005.
[9] J. P. Hindmarsh, D. I. Wilson, and M. L. Johns, 'Using magnetic resonance to validate predictions of the solid fraction formed during recalescence of freezing drops', *Int. J. Heat Mass Transf.*, vol. 48, no. 5, pp. 1017–1021, Feb. 2005.
[10] A. Labergue, J.-D. Pena-Carillo, M. Gradeck, and F. Lemoine, 'Combined three-color LIF-PDA measurements and infrared thermography applied to the study of the spray impingement on a heated surface above the Leidenfrost regime', *Int. J. Heat Mass Transf.*, vol. 104, pp. 1008–1021, 2017.
[11] W. Chaze, O. Caballina, G. Castanet, and F. Lemoine, 'Spatially and temporally resolved measurements of the temperature inside droplets impinging on a hot solid surface', *Exp. Fluids*, vol. 58, no. 8, Aug. 2017.
[12] W. Chaze, O. Caballina, G. Castanet, and F. Lemoine, 'The saturation of the fluorescence and its consequences for laser-induced fluorescence thermometry in liquid flows', *Exp. Fluids*, vol. 57, no. 4, Apr. 2016.
[13] J. Coppeta and C. Rogers, 'Dual emission laser induced fluorescence for direct planar scalar behavior measurements', *Exp. Fluids*, vol. 25, no. 1, pp. 1–15, Jun. 1998.
[14] G. E. Walrafen, 'Raman Spectral Studies of Water Structure', *J. Chem. Phys.*, vol. 40, no. 11, pp. 3249–3256, Jun. 1964.
[15] E. V. Efremov, F. Ariese, and C. Gooijer, 'Achievements in resonance Raman spectroscopy', *Anal. Chim. Acta*, vol. 606, no. 2, pp. 119–134, Jan. 2008.

[16] B. Abramzon and W. Sirignano, 'Droplet vaporization model for spray combustion calculations', *Int J Heat Mass Transf.*, vol. 32, no. 9, pp. 1605–1618, 1989.

[17] D. Duft and T. Leisner, 'Laboratory evidence for volume-dominated nucleation of ice in supercooled water microdroplets', *Atmos Chem Phys*, p. 4, 2004.

[18] G. Castanet, L. Perrin, O. Caballina, and F. Lemoine, 'Evaporation of closely-spaced interacting droplets arranged in a single row', *Int. J. Heat Mass Transf.*, vol. 93, pp. 788–802, Feb. 2016.